

# Design of a Robot-Automated Flat Plate/Reflection Geometry X-ray Diffraction Setup for Accelerated Materials Discovery and Structural Screening

Christopher A. Crain<sup>1</sup>, Kevin H. Stone<sup>1</sup>, Charles Troxel Jr.<sup>1</sup>, Sarah Shulda<sup>2</sup>, David S. Ginley<sup>2</sup>, Nicholas A. Strange<sup>1\*</sup>

<sup>1</sup> *Stanford Synchrotron Radiation Lightsource, SLAC National Accelerator Laboratory, Menlo Park, CA 94025*

<sup>2</sup> *National Renewable Energy Laboratory, Golden, CO 80401*

## **Abstract:**

We report the design, construction, and automation of a flat plate sample loading, alignment, and data acquisition system for X-ray diffraction measurements in reflection geometry implemented at the Stanford Synchrotron Radiation Lightsource. The system is built onto a single platform, enabling facile transferability, and is compartmentalized into sample storage, sample transfer, and sample position/alignment segments. The core feature of this system is a six-axis robotic arm that offers a large range of highly reproducible and programable movements. The degrees of freedom of the robot arm enable adaptability in which movements can be modified to fit various beamline environments and sample configurations. Samples are housed on 3D printed sample mounts, which are arranged onto a  $6 \times 2$  array of sample cassettes capable of holding 7 samples. Using sample mounts designed for solid oxide electrolysis button cells (SOECs), the maximum tray capacity is 84 samples, which can be aligned and run in approximately 24 hours with long exposure scans. The sample array is additionally capable of accommodating a range of sample sizes and geometries due to the rapid 3D printed fabrication. The components of the setup will be described in detail and performance will be demonstrated with a set of representative SOEC and XRD standard samples. Opportunities for future developments and integration with the automated setup are summarized.

## Introduction

A critical need for rapid development of sustainable energy technologies, necessary to reduce costs and enhance deployment of clean and renewable power sources, has motivated several research sectors (e.g., batteries, hydrogen, solar, carbon capture, etc.) to accelerate the materials discovery and performance characterization steps of the research and development cycle. The short timescales for elevating energy production or storage processes and materials to deployment stages has been largely motivated by ambitious decadal cost and performance targets and the urgency of attaining a sustainable energy infrastructure. Automation is a natural solution to significantly enhance the throughput of material structural characterization, given the recent developments and commercial availability of robotic hardware, combined with the advancements of artificial intelligence/machine learning to optimize workflows.

A secondary approach to reducing the time constant of materials characterization is using an optimal source probe, which is achievable with the high flux available at a synchrotron X-ray facility. X-ray scattering and spectroscopy techniques from sources with high brilliance can provide great insight into hierarchical structures, chemical compositions, and degradation pathways of materials. High X-ray energies enable measurements on samples in their native/as-received form (e.g., SOEC button cells, battery coin cells) with little or no sample preparation.

Despite the advantages of synchrotron X-rays, accessibility can be a major hurdle in performing unique structural measurements and acquiring high-quality data at large user facilities. With the annually growing rate of users at DOE-BES user facilities<sup>1</sup> such as the Stanford Synchrotron Radiation Lightsource (SSRL), X-ray beamlines are routinely oversubscribed and user backlogs are developed, a problem common to all user facilities. Consequently, some additional advantages of the availability and development of robotic capabilities at user facilities

include far superior facility efficiencies, standardized/optimized quality of data, and more facile access for new/existing users.

To overcome these challenges, we have designed a robot-automated flat plate/reflection geometry setup for high-throughput X-ray diffraction (XRD) at SSRL beamline 2-1. The automated system can change between samples in seconds without the need for user intervention and incorporates many elements of data collection operations to behave analogous to (or better than) manual alignment and data acquisition scans. Computer controlled sample changing systems capable of operating independently enable greater efficiencies of data collection and are a prerequisite for autonomous X-ray measurements. However, such systems are few in number, are typically not highly versatile in the types of samples they can accommodate, and are largely focused on structural molecular biology.<sup>2-10</sup> The setup described below was designed specifically for rapid XRD data acquisition and analysis of solid oxide electrolyzer button cells (SOECs) but is readily adaptable to many sample form factors given the 3D printed design and manufacture of sample stages. Furthermore, the entire system was designed on an optical breadboard which can easily be transferred across the facilities and integrated on adjacent beamlines with additional measurement capabilities.

### **Description of Components**

The system described herein was designed to automate sample storage, transfer, positioning/alignment, and XRD data acquisition of flat-plate materials. A python script is used to integrate all processes associated with sample manipulation, robot movement, beamline control, and data acquisition into a unified workflow. The setup was developed based on a template described previously for transmission XRD measurements in capillaries at SSRL.<sup>11</sup> The hardware of the current flat plate setup can be compartmentalized and described by three primary

components: sample storage, sample transfer, and sample positioning which are described more fully in the following sections.

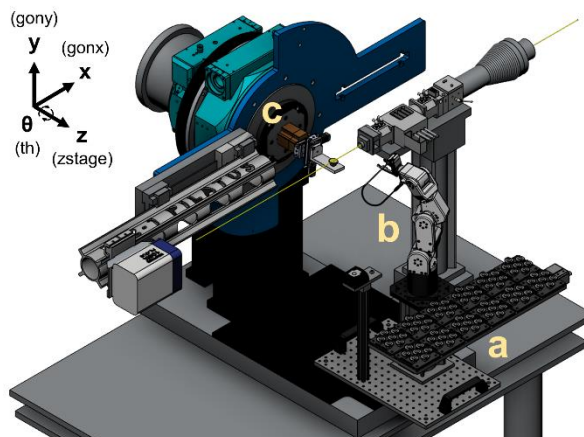


**Figure 1.** Overview of the robot-automated flat plate/reflection geometry setup separated into a) sample storage, b) sample transfer, and c) sample positioning and alignment components. X-rays enter the hutch from right and are diffracted onto the area detector mounted on the two-theta arm shown on the left side of the figure. The right hand-coordinate system is shown for reference in addition to the corresponding sample stage motor initialism.

### *Sample Storage*

All samples, regardless of size/shape, are stored on sample mounts (Figure 2, bottom right) which are magnetically secured to a “cassette” (Figure 2, top right). Sample geometry plays a large role in defining the maximum sample capacity. For the case of SOEC button cells, seven mounts fit in a close-packed configuration on each cassette. A  $6 \times 2$  array of cassettes is affixed to an  $8 \times 24$ ” aluminum optical breadboard (Thorlabs MB824 aluminum breadboard), providing a maximum SOEC capacity of 84 samples per tray (Figure 2, left). All sample mounts and cassettes were 3D printed on a Markforged Onyx machine using a composite filament of nylon and chopped carbon fiber (Markforged F-MF-0001) with a 0.1 mm layer height. The sample mounts were designed to be reproducibly positioned on the cassettes using truncated pyramidal bases, which contain black oxide steel alloy set screws (6-32,  $\frac{1}{4}$ ”). The set screws serve as a ferromagnet mate

to sample mounts containing inset neodymium permanent magnets. The sample mounts contain a concave counterpart to the pyramidal bases with a 0.175 mm clearance gap to yield reproducible and fixed sample positioning. The modified pyramidal shape of the mounting system was designed as a guide to provide the same orientation within the sample surface plane, while restricting rotation after coupling. The pyramidal interface between sample mounts and cassette bases is uniform across all sample form factors; however, the stage component of the sample mount can be customized to any size/geometry as exemplified in Figure 2. In the standard configuration, Each sample mount contains a unique quick response (QR) code, used for positional tracking and capture of metadata associated with each sample. The unique identifier (a 5-digit number) is read into the filename structure which allows for integration with databases which can track sample “chain of custody.”

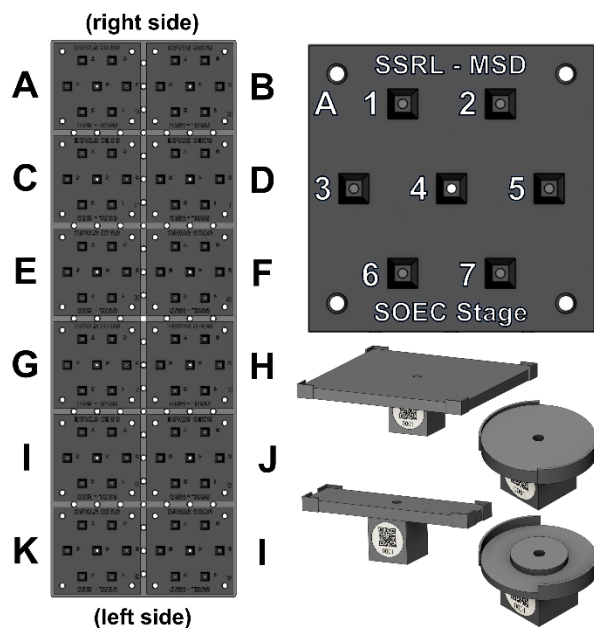


**Figure 2.** Schematics of the cassette array mounted on the sample tray (left), an individual cassette with seven mounting positions (top right), and example SOEC button and planar (i.e. large format) cell sample mounts (bottom right). Each cassette is ordered on the tray and labeled with a letter. Positions within a given cassette are numbered.

### *Sample Transfer*

Sample transfer is handled using a six-axis industrial robot arm (Mecademic Meca500). The robot arm is interfaced to the instrument PC using a local area network connection and operated using a python script that utilizes the Mecademic Python API module<sup>12</sup>, NumPy<sup>13</sup>, and SciPy<sup>14</sup>. The Meca500 web interface can also be used to easily program new poses that are within the workspace. The arm has a positional reproducibility of 0.005 mm and a 260 mm reach for a reasonably sized workspace, but compactly fits inside the beamline hutch without interfering with other equipment. Given the finite range of motion of the robot arm, a 600 mm linear stage (ZABER LSQ600B-E01CT3A-MC10T3) is used to translate the sample mounts within reach of the robot arm during sample transfers. Cassettes which hold the sample mounts are attached to the optical breadboard, which is fastened to the translational stage using a kinematic mount for easy removal and placement. Control of the motor is achieved using a single axis of a multi-axis Galil stepper controller, and locations of cassette positions are programmed into the python script. As seen in Figure 1, the translational stage is attached to the side of the robot pedestal. Because the samples are spaced symmetrically on each cassette, the robot is only indexed to the center sample position of each cassette within a row on the breadboard.

An electric gripper (Mecademic/SCHUNK MEGP 25E) outfitted with forceps allows the robot to capture each sample by latching onto the edges as well as the sides of the sample mounts. The forceps, shown in Figure 3, were 3D printed with carbon fiber-nylon composite filament to add strength. 3D printing the gripper forceps enables simple and rapid fabrication of complex patterns (embedded into the forceps design) which can accommodate a large range of sample footprints.

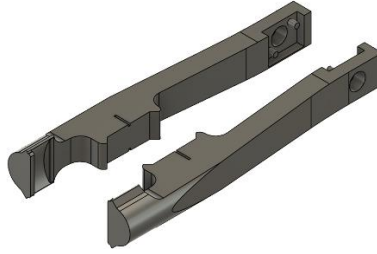


**Figure 3.** Schematic of the 3D printed forceps.

A 3D printed intermediate sample platform is used to adjust the orientation of the sample mounts within the forceps in addition to reading the sample identifier (QR code) using a barcode reader (Zebra DS457).

### *Sample Positioning*

The sample measurement stage is machined from aluminum and is cantilevered to a ZABER motor stack with five axes of motion ( $x$ ,  $y$ ,  $z$ , theta-arc [ $xz$  plane], chi-arc [ $yz$  plane]). The sample motor stack is mounted on a two-circle Huber goniometer, which enables two concentric axes of motion (theta [sample incident angle], two-theta [diffraction angle]) about the  $z$  axis for the standard configuration XRD geometry at SSRL beamline 2-1. Only the sample vertical ( $y$ ) and theta motors are allowed to move during the automated sample alignment procedure. The aluminum sample stage contains a machined pyramidal base identical to those on the cassettes.

### **System Operation**

Operation of the robot-automated setup was designed to require as little interaction as possible necessary to perform continuous flat plate/reflection geometry XRD measurements. Preliminary steps such as sample preparation and positioning of the entire system still require minimal user intervention. Sample preparation entails placing samples on the 3D printed sample mounts and positioning the holders onto the cassettes sequentially with the QR code facing towards

the center of the tray. Once the robot is connected to the control PC and initialized, the hutch is secured, ending user interaction with the system hardware.

A python script is utilized for automated control using subroutines to manipulate the sample positioning within the workspace, create data directories and filenames from the QR codes, perform height and incident angle alignments using the incident X-ray beam, and control XRD data acquisition, all while informing any observer of the current status through a text-based console. The script was developed to control SSRL beamline 2-1 which uses the SPEC software package<sup>15</sup> for positioning/alignment operations and data collection. However, such a self-contained system can be adapted for other SSRL beamlines, user facilities, or characterization techniques, provided these steps can be input through a command line interface.

When the python control script is initially executed, the current positions of the sample motors (y [gony], z [zstage], and theta [th]) are requested for homing during sample changes, in addition to the number of samples to run. After the input is confirmed, the control script supersedes the user as the operator and establishes a connection to the robotic arm.

A “sample loading” routine controls the positions of the sample tray relative to the robotic arm. Initially, the linear stage is driven to the first sample cassette (A in Figure 2), which is centered directly in front of the robotic arm. The 14 sample positions within a given row (e.g., AB) are mapped such that sample positions in adjacent rows (e.g., CD, EF, HI,...) can be exactly replicated by a translation of the linear stage. The script directs the robotic arm to the first sample mount (A1). Upon capturing the sample mount in the forceps, the arm lifts and reorients to the intermediate sample stage. A “QR code” subroutine is called to scan the sample and create directories for alignment and measurement files based on the unique sample identifier. The robot

arm then picks up the sample mount from the side and positions the sample on the sample measurement stage.

The python script then executes a “sample alignment” routine, consisting of three iterations of alternating sample vertical (y) and incident angle (theta) alignments prior to the full data acquisition scan. Subsequent iterations of the alignment procedure utilize narrower bounds of motion, providing finer binning and more accurate alignments. Initial scan parameters are intentionally coarse to account for variations in sample thickness and roughness between samples. Successful completion of the automated alignment procedure enables positional reproducibility as demonstrated by figure S1.

A “data acquisition” subroutine sets the incident angle of the aligned sample and performs angle-resolved XRD measurements saving the data files to the paths specified by the QR code subroutine. Upon completion of data collection, the robotic arm removes the sample from the sample measurement stage, re-oriens using the intermediate sample stage, and places it back onto the cassette position of origin. As a quality control step, the robot scans the sample mount removed from the beamline using the barcode reader. This process is repeated for the subsequent sample position(s) in the current and remaining cassettes. Upon completion of the final sample, the robotic arm is returned to a resting position and the connection is disabled.

Unexpected positioning errors can arise due to a failure involving either the forceps or the magnetic sample mount, both of which cause the robot to stand down to prevent the loss of additional samples. In the event of a sample location error flagged by the QR code subroutine, quality control measures are implemented to prevent erroneous motions of the robot arm which could damage the sample(s) or beamline components. If the barcode reader does not detect a QR code after two minutes of failed attempts, the script halts all motions and prompts, “Is there a

sample in the forceps?” to which the operator can input Y (yes), N, (no), or Q (quit). “Yes” enables the robot to continue attempting to read in the sample identifier, whereas “no” prompts the robot arm to move the next sample in the queue and write a file to note the error in the procedure. Commanding “quit” discontinues operations and moves the robot arm into its idle position.

## **System Performance**

The automated sample changing system described above is a powerful tool for enabling high throughput flat-plate measurements at material characterization facilities and can run independent of user interaction from several hours to a day under optimal circumstances. The system performance is demonstrated below with output from the automated alignment procedure as well as example data from standard materials and SOECs.

### *Automated Alignment*

As noted previously, the automated alignment procedure involves three iterations of alternating sample vertical and incident angle alignment scans intended to calibrate the positions to zero. Initially, the sample is mounted with the surface plane nominally parallel with the incident beam. The sample vertical alignment scan translates the approximately flat sample through the direct beam from a low to high position. The observed direct beam intensity, as recorded by an in-line photodiode, decays as a sloped step function as the sample intersects the beam path as observed in Figure 3. The numerical derivative of this sloped profile is obtained (dashed profile in Figure 3) and the minimum value of the derivative is chosen as the middle of the slope (i.e., the top of the sample surface plane). Subsequently, an incident angle alignment scan is performed whereby the incident angle is rotated from  $-4$  to  $+4^\circ$  about the nominally flat position. As this motion proceeds, the direct beam intensity displays a peak function (pointed for smooth surfaces

and smeared into a bell-shaped curve for rough surfaces). The first iteration of these scans is a coarse alignment, utilizing broad spans of motion, which accounts for natural variations in thickness and flatness from sample to sample. The second and third iterations of the alignment procedure narrow the bounds of motion (thereby increasing resolution) to converge on the most appropriate sample positions.

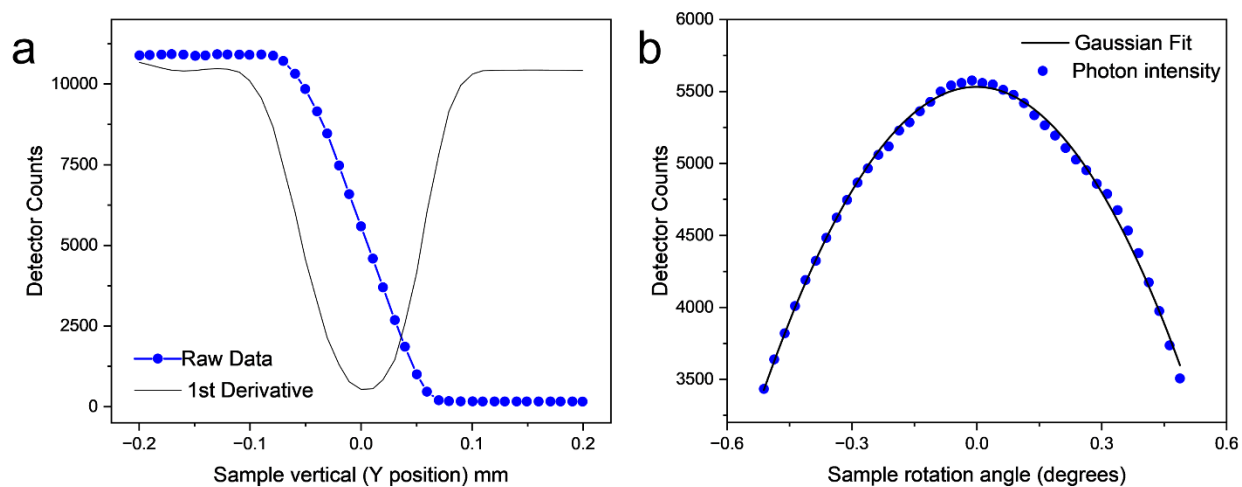


**Figure 4.** Example (a) sample vertical and (b) incident angle alignment scans from an SOEC.

### *Data Acquisition*

Ten standard samples were run to demonstrate sample throughput and quality of data. The samples included a sintered alumina plate (NIST 1976b), yttria-stabilized zirconia (YSZ) substrate, tantalum (Ta), tungsten (W), and platinum (Pt) metal foils, lanthanum hexaboride ( $\text{LaB}_6$ ), a titanium oxide ( $\text{TiO}_2$ ) pressed pellet, and four SOEC button cells (Nexceris). A selection of the XRD results is shown below in Figure 2, demonstrating the high signal-to-noise and resolution of the instrument and measurement configuration. The complete set of data and video (Multimedia available online) of the procedure are provided in the supplementary information (see Figures S2-S12).

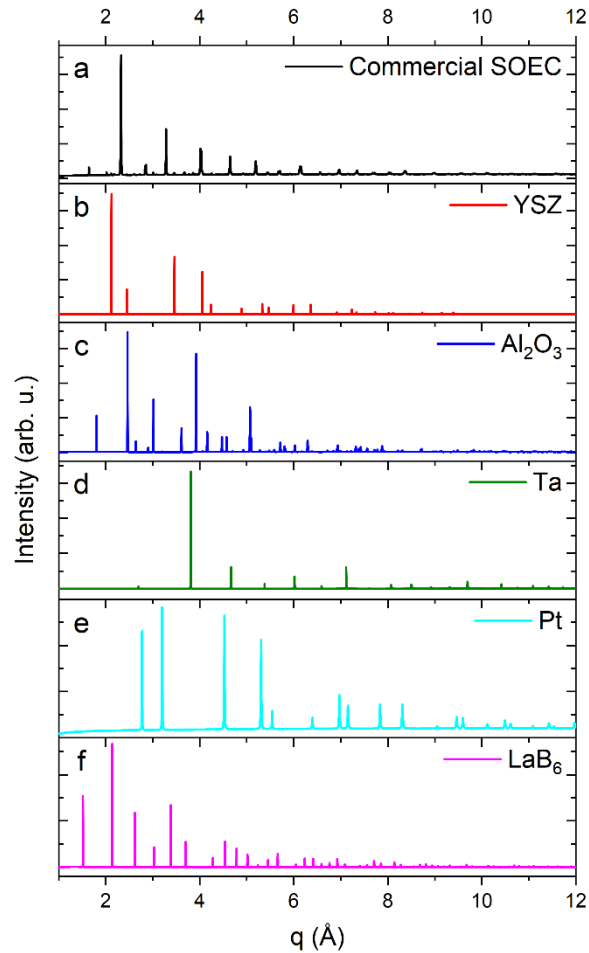


**Figure 5.** XRD data from standard samples, including a (a) commercial SOEC, (b) yttria-stabilized zirconia (c) sintered alumina, (d) Ta, and (e) Pt metal foils, and a (f) LaB<sub>6</sub> plate.

### Future Developments

There are several developments that can be incorporated to expand the utility of the system. Of primary importance is expanding the ability to control measurement conditions including geometries (symmetric vs. asymmetric reflection), scan parameters (angular limits, exposure time), variable incident angles, and sample rocking. Selection and input of measurement conditions can be streamlined using a sample spreadsheet with keywords, which can be read into the python script. Secondly, adding the ability to perform spatial mapping would enable the determination of structural heterogeneities in large format samples, such as planar SOECs. Additionally, we envision a Si-drift (Vortex) detector will be implemented parallel to the beam path to enable

simultaneous elemental analysis based on X-ray fluorescence. In principle, the entire tray-mounted robotic setup could be translated to any SSRL beamline or technique, provided the tray can be secured and the flat plate sample geometry is compatible with the technique. X-ray absorption spectroscopy with fluorescence detection and grazing-incidence small angle X-ray scattering are promising candidates for cross-technique implementation.

Beyond the developments outlined above, there are further opportunities to integrate our setup with external resources to further enhance the utility. Our unique sample identifier can be used with sample databases<sup>3</sup> to associate any metadata (i.e., synthesis conditions, batch number, processing, etc.), lab-based characterization, multi-scale modeling, or measurements from other large scale user facilities (e.g., X-ray, neutron, electron microscopy). In the interest of moving further towards fully autonomous systems, it may be valuable to integrate artificial intelligence/machine learning<sup>16</sup> with the robot-automated setup to accelerate the sample alignment, data acquisition, processing, and analysis steps.

## **Summary**

The design and fabrication of a setup for automated flat plate/reflection geometry XRD measurements at SSRL beamline 2-1 has been described. The system is segregated into three components, namely sample storage, sample transfer, and sample positioning/alignment. The sample mounts were initially designed for SOEC button cells but can be readily adapted to nearly any sample form factor using 3D printing for mount fabrication. We have detailed the operation procedure, presented example data sets from the automated alignment routine, and XRD data from representative samples. This capability enables rapid sample throughput, necessary for accelerated material discovery and characterization, applicable to many modern applied research topics

including hydrogen production, batteries, and photovoltaics. A number of future developments and opportunities to integrate with offline components have been presented as next steps.

### **Supplementary Material**

The supplementary material contains a description of the XRD experimental configuration and parameters, a figure illustrating the reproducibility of the automated alignment algorithm (Fig. S1), ten XRD patterns from representative classes of materials obtained using the flat plate automated robot system (Fig. S2-S11), and a video demonstrating the automated sample manipulation, alignment, and acquisition procedures (Fig. S12).

### **Acknowledgments**

The authors would like to acknowledge the financial support from the U.S. Department of Energy's Office of Energy Efficiency & Renewable Energy, Hydrogen Fuel Cell Technology Office through AOP 12.1.0.905 and Memorandum of Purchase Order 23-0068-IE with the National Renewable Energy Laboratory. Use of the Stanford Synchrotron Radiation Lightsource, SLAC National Accelerator Laboratory, is supported by the U.S. Department of Energy, Office of Science, Office of Basic Energy Sciences under Contract No. DE-AC02-76SF00515.

### **Data Availability Statement**

The data that support the findings of this study are available within the article and its supplementary material.

### **References**

<sup>1</sup> U.S. Department of Energy Office of Science, "Number of Users Reported by BES User Facilities," (2022), [https://science.osti.gov/-/media/bes/suf/pdf/BES\\_Facilities\\_Number\\_of\\_Users.pdf](https://science.osti.gov/-/media/bes/suf/pdf/BES_Facilities_Number_of_Users.pdf).

- <sup>2</sup> C.A. Smith, G.L. Card, A.E. Cohen, T.I. Doukov, T. Eriksson, A.M. Gonzalez, S.E. McPhillips, P.W. Dunten, I.I. Mathews, J. Song, and S.M. Soltis, “Remote access to crystallography beamlines at SSRL: novel tools for training, education and collaboration,” *J. Appl. Crystallogr.* **43**(5), 1261–1270 (2010).
- <sup>3</sup> E.O. Lazo, S. Antonelli, J. Aishima, H.J. Bernstein, D. Bhogadi, M.R. Fuchs, N. Guichard, S. McSweeney, S. Myers, K. Qian, D. Schneider, G. Shea-McCarthy, J. Skinner, R. Sweet, L. Yang, and J. Jakoncic, “Robotic sample changers for macromolecular X-ray crystallography and biological small-angle X-ray scattering at the National Synchrotron Light Source II,” *J. Synchrotron Rad.* **28**(5), 1649–1661 (2021).
- <sup>4</sup> N. Okazaki, K. Hasegawa, G. Ueno, H. Murakami, T. Kumasaka, and M. Yamamoto, “Mail-in data collection at SPring-8 protein crystallography beamlines,” *J. Synchrotron Rad.* **15**(3), 288–291 (2008).
- <sup>5</sup> A.S. Losko, S.C. Vogel, H.M. Reiche, and H. Nakotte, “A six-axis robotic sample changer for high-throughput neutron powder diffraction and texture measurements,” *J. Appl. Crystallogr.* **47**(6), 2109–2112 (2014).
- <sup>6</sup> G.J. Havrilla, and T.C. Miller, “High-throughput screening with micro-x-ray fluorescence,” *Rev. Sci. Instrum.* **76**(6), (2005).
- <sup>7</sup> Z. Luo, B. Geng, J. Bao, C. Liu, W. Liu, C. Gao, Z. Liu, and X. Ding, “High-throughput x-ray characterization system for combinatorial materials studies,” *Rev. Sci. Instrum.* **76**(9), (2005).
- <sup>8</sup> J.M. Gregoire, D. Dale, A. Kazimirov, F.J. Disalvo, and R.B. Van Dover, “High energy x-ray diffraction/x-ray fluorescence spectroscopy for high-throughput analysis of composition spread thin films,” *Rev. Sci. Instrum.* **80**(12), (2009).
- <sup>9</sup> S. Purushothaman, B.L.L.E. Gauthé, N.J. Brooks, R.H. Templer, and O. Ces, “Automated laboratory based X-ray beamline with multi-capillary sample chamber,” *Rev. Sci. Instrum.* **84**(8), (2013).
- <sup>10</sup> S.Ý. Ágústsson, A.J.H. Jones, D. Curcio, S. Ulstrup, J. Miwa, D. Mottin, P. Karras, and P. Hofmann, “Autonomous micro-focus angle-resolved photoemission spectroscopy,” *Rev. Sci. Instrum.* **95**(5), (2024).
- <sup>11</sup> K.H. Stone, M.R. Cosby, N.A. Strange, V. Thampy, R.C. Walroth, and C. Troxel Jr, “Remote and automated high-throughput powder diffraction measurements enabled by a robotic sample changer at SSRL beamline 2-1,” *J. Appl. Crystallogr.* **56**(5), 1480–1484 (2023).
- <sup>12</sup> Mecedemic, “Mecedemic Python API,” (2023), <https://github.com/Mecedemic/mecedemicpy>.
- <sup>13</sup> C.R. Harris, K.J. Millman, S.J. van der Walt, R. Gommers, P. Virtanen, D. Cournapeau, E. Wieser, J. Taylor, S. Berg, N.J. Smith, R. Kern, M. Picus, S. Hoyer, M.H. van Kerkwijk, M. Brett, A. Haldane, J.F. del Río, M. Wiebe, P. Peterson, P. Gérard-Marchant, K. Sheppard, T. Reddy, W. Weckesser, H. Abbasi, C. Gohlke, and T.E. Oliphant, “Array programming with NumPy,” *Nature* 2020 585:7825 **585**(7825), 357–362 (2020).

<sup>14</sup> P. Virtanen, R. Gommers, T.E. Oliphant, M. Haberland, T. Reddy, D. Cournapeau, E. Burovski, P. Peterson, W. Weckesser, J. Bright, S.J. van der Walt, M. Brett, J. Wilson, K.J. Millman, N. Mayorov, A.R.J. Nelson, E. Jones, R. Kern, E. Larson, C.J. Carey, Í. Polat, Y. Feng, E.W. Moore, J. VanderPlas, D. Laxalde, J. Perktold, R. Cimrman, I. Henriksen, E.A. Quintero, C.R. Harris, A.M. Archibald, A.H. Ribeiro, F. Pedregosa, P. van Mulbregt, A. Vijaykumar, A. Pietro Bardelli, A. Rothberg, A. Hilboll, A. Kloeckner, A. Scopatz, A. Lee, A. Rokem, C.N. Woods, C. Fulton, C. Masson, C. Häggström, C. Fitzgerald, D.A. Nicholson, D.R. Hagen, D. V. Pasechnik, E. Olivetti, E. Martin, E. Wieser, F. Silva, F. Lenders, F. Wilhelm, G. Young, G.A. Price, G.L. Ingold, G.E. Allen, G.R. Lee, H. Audren, I. Probst, J.P. Dietrich, J. Silterra, J.T. Webber, J. Slavič, J. Nothman, J. Buchner, J. Kulick, J.L. Schönberger, J.V. de Miranda Cardoso, J. Reimer, J. Harrington, J.L.C. Rodríguez, J. Nunez-Iglesias, J. Kuczynski, K. Tritz, M. Thoma, M. Neville, M. Kümmerer, M. Bolingbroke, M. Tartre, M. Pak, N.J. Smith, N. Nowaczyk, N. Shebanov, O. Pavlyk, P.A. Brodtkorb, P. Lee, R.T. McGibbon, R. Feldbauer, S. Lewis, S. Tygier, S. Sievert, S. Vigna, S. Peterson, S. More, T. Pudlik, T. Oshima, T.J. Pingel, T.P. Robitaille, T. Spura, T.R. Jones, T. Cera, T. Leslie, T. Zito, T. Krauss, U. Upadhyay, Y.O. Halchenko, and Y. Vázquez-Baeza, “SciPy 1.0: fundamental algorithms for scientific computing in Python,” *Nat. Methods* 2020 17:3 **17**(3), 261–272 (2020).

<sup>15</sup> Certified Scientific Software, “spec<sup>TM</sup> X-Ray Diffraction Software,” ©1989, (2017), <https://certif.com/spec.html>.

<sup>16</sup> N.J. Szymanski, C.J. Bartel, Y. Zeng, M. Diallo, H. Kim, and G. Ceder, “Adaptively driven X-ray diffraction guided by machine learning for autonomous phase identification,” *Npj Comput. Mater.* 2023 9:1 **9**(1), 1–8 (2023).